IL NUOVO CIMENTO **41 C** (2018) 196
DOI 10.1393/ncc/i2018-18196-2

COLLOQUIA: IWM-EC 2018

Upgrade of the experimental Facilities at LNS

D. SANTONOCITO(1), A. CALANNA(1), G. BELLIA(1)(2), R. ALBA(1), A. DEL ZOPPO(1), C. MAIOLINO(1), A. DI PIETRO(1), P. FIGUERA(1), M. LATTUADA(1)(2), L. CALABRETTA(1), A. D. RUSSO(1), P. RUSSOTTO(1)

(1) *INFN, Laboratori Nazionali del Sud - via S. Sofia 62, I-95123, Catania Italy*
(2) *Dipartimento di Fisica e Astronomiá dell'Università di Catania - via S. Sofia 64, I-95123, Catania, Italy*

received 3 December 2018

Summary. — A feasibility study to build an helical orbit spectrometer using the SOLE magnetic field is presented in the more general context of the upgrade project of the LNS facilities. It includes the upgrade of the superconducting cyclotron to deliver high-intensity beams and the design of a new fragment separator optimized to match the beam optics of the secondary beams produced by projectile fragmentation. The main features of a helical-orbit spectrometer together with simulations performed using the SOLE magnetic field are presented and compared to the results obtained using a homogeneous solenoid field. The effects related to the geometry of the detection array and to the beam spot size on the detected impact point distribution and on the recostruction of the emission angle are also discussed.

1. – Introduction

The increasing demand of high intensities beams to study rare processes in nuclear physics has motivated a project of upgrade of the LNS Superconducting Cyclotron (CS). The CS, which has been in operation for more than twenty years, can accelerate a wide range of ion species from H to Pb in an energy range from 10 to 80 A MeV with a maximun beam power limited to 100 W due to the beam dissipation on the electrostatic deflector. The main features of the upgraded machine would allow an increase of beam power to about 10 KW using the extraction by stripping, a technique which could be efficiently used for ion beams with masses up 40 a.m.u. keeping unchanged the present extraction method for all other nuclear species [1]. At the same time the availability of high-intensity beams would also allow to produce intense radiactive ion beams (RIBs) by projectile fragmentation. The performances of the current RIB facility built on the CS and the fragment separator FRIBs [2] did not allow to populate nuclei far from the stability valley with a sizeable yield and for this reason a totally new fragment separator

called FRAISE [3] has been designed. It will represent, together with the CS upgrade one of the pillars of the future LNS facility.

The upgraded machine will open up the possibility to measure cross sections for double charge exchange nuclear reactions which represent the main focus of the NUMEN project [4] at the INFN-LNS and can be used to derive relevant information about the nuclear matrix elements of interest for neutrinoless double-beta decay. To reach this goal a new focal plane detector and a new wall of stopping detectors for the MAGNEX spectrometer [5] are under costruction. Such devices will allow to work with a beam intensity two orders of magnitude higher than the present one, which is needed to reach the NUMEN goal and undertake a systematic study of the "hot" cases of $\beta\beta$ decay.

A new array called FARCOS (Femtoscope ARray for COrrelations and Spectroscopy) [6] has been developed by the INFN Catania (Sezione and LNS) and is now almost completed. This new device aims to perform high precision measurements of two and multi-particle correlations in heavy-ion collisions at intermediate energies ($E = 20$–$100\,A$ MeV). Coupled to CHIMERA 4π detector [7], it will allow to extend the studies of reaction dynamics at intermediate energies and the investigation of the equation of state properties in asymmetric nuclear matter using exotic beams.

The availability of exotic beams produced by projectile fragmentation with FRAISE will also open up new possibilities to investigate the nuclear structure and measure the basic properties of nuclei at the extremes of stability valley such as the shell evolution and their collective phenomena. Such studies tipically require both, high-efficiency detector arrays and high cross section reactions, due to the beam intensities that can be as low as 10^4 pps. Direct reactions represent the tool of choice as they allow to infer basic properties of the investigated nuclei: elastic scattering can probe protons and neutrons density distributions, inelastic scattering can probe collective aspects, and transfer reactions allow to get information on single particle states and pair correlation. The necessity to use inverse kinematics, in the case of RIBs, introduces some experimental problems both in the identification of low-energy particles emitted in such kind of reactions and in the angular resolution, since the strong focusing of products in a limited angular region tends to reduce the achievable separation among the excited states. To overcome such difficulties a helical-orbit spectrometer could be implemented and play an important role in the experimentation due to its high efficiency and high resolution. In the last few years a feasibility study to build a helical-orbit spectrometer using the magnetic field of SOLE solenoid [8] has been undertaken. It is presently coupled to MEDEA detector array [9] and it is used to focus the evaporation residues populated in complete and incomplete fusion reactions on the focal plane detector MACISTE [8]. In the following, a short description of the FRAISE fragment separator will be given. Then the helical-orbit spetrometer main features will be presented together with the preliminary results of this study.

2. – The fragment separator FRAISE

The increase in beam power of the new CS, for ions up to mass $A = 40$, allows a sizeable improvement in the intensities of secondary beams achieved by the in-flight separation technique. The key instrument of every in-flight facility is the fragment separator, namely a magnetic filter that selects the produced fragments accordingly to their magnetic rigidity. In the present configuration it consists of two bending dipoles, three quadrupole triplets and two sestupole correctors placed near quadrupole elements. A 250–1500 μm thick beryllium production target, is placed at the exit of the

CS extraction line which is used as achromatic fragment separator. A degrader can be placed at the intermediate focus, between the two dipoles to improve the selections of the ion species produced.

Due to radioprotection costraints the existing fragment separator cannot operate with high power beams. Therefore a new fragment separator, named FRAISE (FRAgment In-flight SEparator), was designed and optimized to match the profile of the secondary beams produced. It will be placed in the area where are presently located the 20° and 40° LNS experimental rooms to maintain the possibility to deliver the beams in the largest possible number of experimental areas as shown in fig. 1. In this new configuration, according to the simulations performed, up to 2 kW of primary beam power can be safely used.

FRAISE consists of two parts, the second one being a mirror-copy of the first one. It is composed by two 70° and 40° dipoles (D1–D4 and D2–D3, respectively), 6 quadrupoles (from Q1 to Q6) and 3 sestupoles as shown in fig. 1. This design ensures a full achromaticity of the fragment separator. Since the spectrometer cannot separate ions having

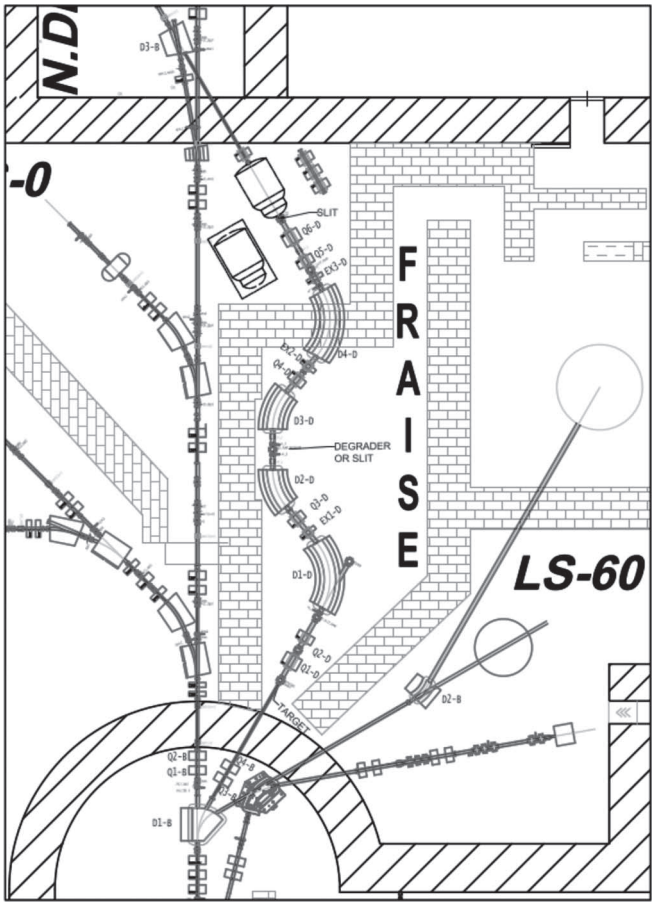

Fig. 1. – Layout of the new fragment separator FRAISE placed in the area where are presently located the 20° and 40° LNS experimental areas. The exit beam line (top part of the figure) is used to deliver beams in the MAGNEX and CHIMERA experimental areas.

TABLE I. – *Expected fragment yields combining the beam intensities of the CS upgraded with the performances of the new fragment separator FRAISE.*

Fragment	Primary beam and energy (A MeV)	Thickness Be target (μm)	Wedge thickness (μm)	Primary intensity (kW)	Expected yield (kHz)	Purity (%)	Energy after tagging (A MeV)
^{14}Be	^{18}O/55	1500	0	2	2.6	2	46
^{14}Be	^{18}O/55	1500	1000	2	2.2	70	43
^{13}N	^{16}O/40	700	600	2	1230	54	4
^{14}O	^{16}O/40	700	600	2	807	36	4
^{18}Ne	^{20}Ne/60	1000	0	2	16700	16	43
^{18}Ne	^{20}Ne/60	1000	1000	2	3120	47	24
^{17}F	^{20}Ne/60	1000	1000	2	3300	49	23
^{34}Si	^{36}S/40	500	500	2	980	81	11
^{38}S	^{40}Ar/40	500	300	2	1840	66	17
^{34}Ar	^{36}Ar/50	250	0	2	2800	4	41
^{34}Ar	^{36}Ar/50	250	500	2	426	12	4
^{68}Ni	^{70}Zn/50	250	200	1	490	50	18

the same A/q ratio, on the symmetry dispersive plane there will be the possibility to insert a degrader, wedge shaped, which slows down the fragments as a function of their atomic number and velocity allowing for a better separation in the second dispersive stage. A proper tuning of the magnetic field in the second part of the spectrometer, after the wedge, allows to select nuclei of a given A^3/Z^2 [10]. A slit system will be inserted on the symmetry plane to provide a mechanical control of the beam profile while a second slits system, placed at the exit of the fragment separator, will allow for a further shaping of the beam profile and improve the isotopic selection. FRAISE will have a selectable momentum acceptance up to a $\Delta p/p \sim \pm 1.2\%$, with a gain of a factor of five compared to the present fragment separator and it is expected to deliver higher purity beams with a proper use of the slits systems and the wedge. Few examples of secondary beam intensities calculated using the LISE simulation code [11] are given in table I. In the same table, the primary beam energy and intensity, production target thickness, wedge thickness, beam purity and final beam energy are listed to provide a more complete description of the performances of the fragment separator.

In the configuration described above the FRAISE fragment separator will only deliver high-intensity RIBs to MAGNEX and CHIMERA experimental areas. Solutions are under investigation to extend RIBs delivery using, for example, a second arm of FRAISE towards the already existing CICLOPE multi-purpose scattering chamber and re-locate on another beam line the SOLE superconducting solenoid [8] to be used as a stand-alone device operating in a configuration similar to the one of the HELIOS spectrometer at Argonne [12, 13], as discussed below.

3. – The helical-orbit spectrometer

The LNS are equipped, since many years, with a superconducting solenoid called SOLE, placed downstream the MEDEA scattering chamber, which has been used to focus

evaporation residues populated in complete and incomplete fusion reactions on the focal plane detector MACISTE placed 16 m downstream the target. The SOLE solenoid is 2 m long with an inner radius of 30 cm for beam transport and can generate a magnetic field up to 5 T. Such a device has the main features in terms of dimensions and magnetic field intensity suitable to investigate its use as a light-charged-particle spectrometer following the HELIOS scheme at Argonne [13].

3˙1. *The concept.* – The basic idea, developed in HELIOS spectrometer, is to use a large bore solenoid with a highly omogeneus field. Heavy-ion beams enter in the solenoid aligned with the magnetic axis and impinge on a target placed inside the solenoid. The light charged particles emitted in a two-body reaction follow helical trajectories inside the solenoid volume and, if the maximum distance from the magnetic axis does not exceed the solenoid radius, they are focused back on the solenoid axis where they can be detected using a hollow array of position-sensitive silicon detectors. This array measures the particle impact point (z), its energy (E_{lab}) and time of flight (ToF). From the energy and impact point measurement it is possible to derive the particle energy in the center-of-mass $E_{c.m.}$ and the emission angle $\theta_{c.m.}$.

The working principle of a helical-orbit spectrometer provides some advantages compared to more traditional detection approaches. In particular, it allows, in an simple way, particle identification overcoming the problem of low-energy particle identification (energy threshold). In a homogeneous field and assuming that relativistic corrections are small, the time of flight corresponds to the cyclotron period, *i.e.*, the time needed to travel a single orbit, given by the relation

$$T_{cycl} = 65.6 \times A/qB\,(\mathrm{ns}), \tag{1}$$

where A is the mass number in a.m.u., B is in T and q is in units of e [13]. Assuming a B value of 2–3 T, the T_{cycl} for protons, alphas, tritons differ by several tens of nanoseconds allowing for an easy separation in ToF and identification while deuterons and alphas have the same ToF. Besides, the detection in (E, z) shows no kinematical compression effects typical of inverse kinematics reactions and a large geometrical acceptance with a limited number of detectors and electronics can be easily reached. For a fixed position z along the magnetic axis, corresponding to a fixed emission angle from the target, a detection array with square or exagonal cross section has a geometrical acceptance close to 2π giving a sizeable advantage compared to more traditional approaches when low cross-sections or beam intensities are involved.

3˙2. *The trasport simulations.* – The magnetic field of LNS superconducting solenoid, built to convey the reaction products of intermediate energy heavy ion collisions on a focal plane detector MACISTE, has not the same degree of homogeneity as the magnet used in HELIOS. Therefore to explore the possibility to use SOLE a wide set of simulations to study the main features of an helical orbit spectrometer built on the SOLE field was performed.

The first step was the creation of a detailed SOLE field map for different values of the current in the solenoid coils. This was accomplished using the code OPERA [14] which generates a field map once the geometry of the solenoid coils and iron distribution are properly introduced. The results were validated through a comparison with the values of the SOLE axial and radial field measured in past. The shape of the axial field for a coil current generating a 2 T field in the center of the solenoid is shown in fig. 2(a). The field

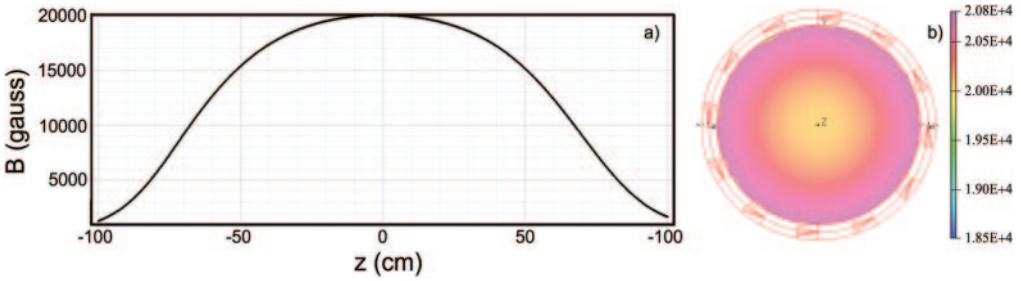

Fig. 2. – (a) Axial profile of the magnetic field along the whole solenoid. (b) Radial profile of the magnetic field taken at $z = 0$ (center of the solenoid).

profile shows a marked variation along the axis with a reduction of the field intensity of about 25% in a quarter of the solenoid length (50 cm) from the center while at about 20 cm the reduction is about 3%. Radially the variation is less pronounced being of the order of 4–5% as shown in fig. 2(b).

Using the field map generated in OPERA we started studying the motion of the light charged particles emitted from a target placed along the magnetic axis to evaluate the distance they return to the axis, the maximum distance reached from the magnetic axis during the motion and their time of flight. Simulations were run for different values of the magnetic field, particle energy and emission angle from the target.

In order to evaluate the effect of the magnetic field profile on the quantities simulated, two different positions of the target were explored, one in the center of the magnet and the other placed at -20 cm from the center to use a larger region of homogeneous field in the case of forward emission (see fig. 2(a)). The results obtained in the case of 6 MeV protons emitted in the forward direction in a field of 3 T are show in fig. 3 as an example. Figure 3(a) shows, as green square symbols ($Z = 0$ ideal), the distance from the target reached by the proton once it returns to the magnetic axis in the case of an ideal homogeneos solenoid field. As a comparison the distance from the target reached by the proton in the case of a target placed at $z = -20$ cm and at $z = 0$ are shown

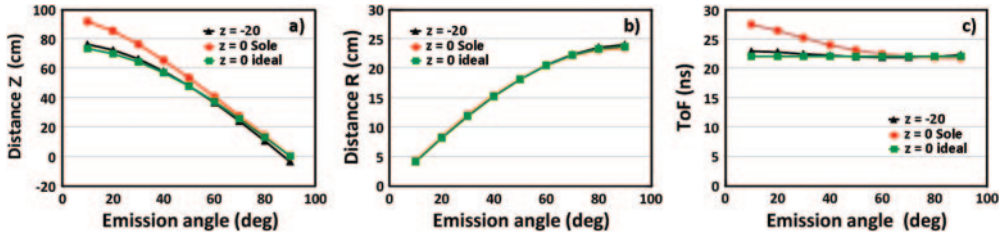

Fig. 3. – (a) Distance travelled by 6 MeV protons, emitted from the target, along the helical trajectory to return to the magnetic axis as a function of emission angle. Results obtained using a 3T solenoidal homogeneous field are compared to SOLE field (3T at the center) for two different target position along the magnetic axis. (b) Maximum radial distance from the magnetic axis reached by the protons during their motion in the magnetic field as a function of emission angle. Symbols correspond to the simulations shown in (a). (c) Time of flight for the different magnetic fields and target configurations as shown in (a) are presented as a function of the emission angle.

as black triangles and red full circles, respectively. While at large emission angles the difference in the travelled distance between the two target positions is small, due to the fact that the proton motion is confined in a region where the magnetic-field variation is small, for small emission angles the travelled distance is much larger and the protons explore a region of reduced magnetic field being less focused than in the ideal case. The simulations using a target at $z = -20$ cm show results closer to the ideal case compared to the simulations with target at the center. The observed differences are energy dependent and increase with the energy when comparisons are made at fixed emission angle. The results concerning the maximum distance from the magnetic axis reached by the protons as a function of the emission angle are displayed in fig. 3(b). Small differences are observed between the different positions of the target and the ideal case. Proton times of flight for the different configurations are presented in fig. 3(c) and compared to the ideal case of homogeneous field. A small dependence as a function of the emission angle is observed using SOLE field, differently from what is predicted in an homogenous field. Such an effect would not affect the particle identification, the time difference among particles being much larger than the observed ToF angular dependence. The results clearly indicate an advantage in the focalization properties using the configuration with the target placed at 20 cm from the center and therefore the simulation that will be presented in the next part of the paper are performed accordingly.

The LNS RIBs are produced by in flight technique and therefore a fundamental issue to investigate is how the spectrometer performances are influenced by the beam spot size. In order to study this dependence, simulations were run assuming protons of energies ranging from 1 to 15 MeV, a wide range of polar emission angles and different beam spot sizes. A detection array geometry with a square cross section of 20 mm lenght was assumed in the calculations. To reproduce, in a simple way, the effect of the beam size on the detector impact points, we assumed the emission from 8 points, 45° spaced along a circumference whose radius corresponds to the beam dimension on the target. For each of these points, the emission of protons with fixed energy and polar angle was assumed while the azimuthal angle was let to vary from 0° to 360°. This simple approach allowed us to follow the evolution of the impact point distance as a function of the azimuthal angle. A spread in the impact point distance is observed reflecting the geometry of the array and the different distances from the emission axis where the proton hits the detector. Figure 4 shows the results for 4 MeV protons emitted at $\theta = 70°$ and $\theta = 70.5°$ polar angles. Each color line corresponds to one emission point. A beam spot size of 2 mm radius was used in the simulations. Emission points inside the circle would give rise to a smaller spread in space. Two well separated regions each corresponding to the spread of impact points along the detector (in the z-direction) can be observed indicating that the spectrometer is able to easily separate trajectories with half a degree difference. The results are energy and polar angle dependent.

In order to study angular distribution for transitions to different excited states is mandatory to be able to separe the states and measure angle and energy with high accuracy. A helical-orbit spectrometer like HELIOS measures particle energy and its impact position along the magnetic axis which are then used to infer the emission angle. In this feasibility study we tried to evaluate, through simulations, the indetermination in the angle reconstruction and how it is linked to the beam size once the particle impact point on the detector is known. This is not an easy task in a not homogeneous magnetic field due to the fact that if one detects the impact point only along the z-axis actually selects a region of impact points that depends on the transversal extent of each detector (in our simulation 20 mm). A significant improvement in the angle reconstruction is

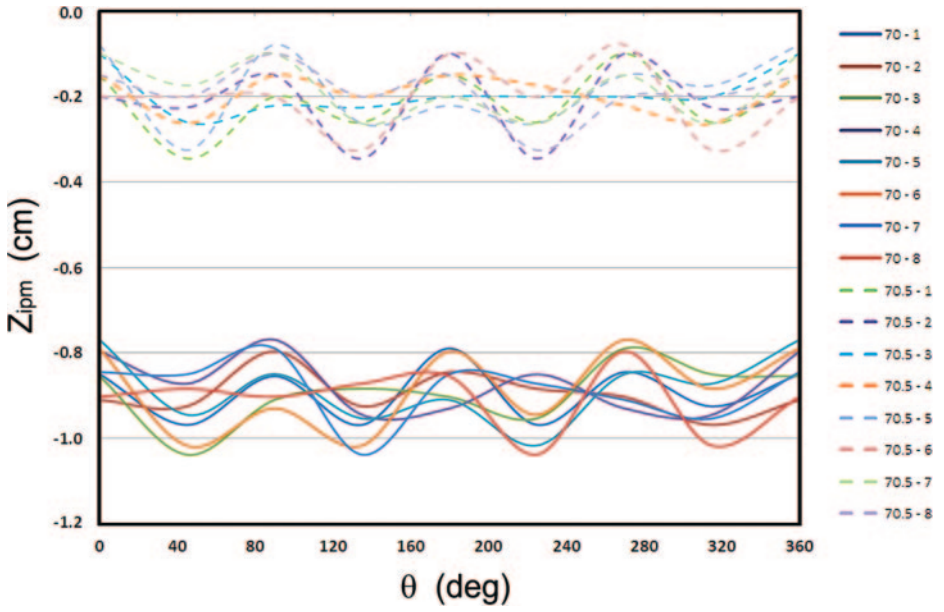

Fig. 4. – Evolution of the impact point on the detector array for 4 MeV proton emitted at $\theta = 70^\circ$ and $\theta = 70.5^\circ$ as a function of azimuthal emission angle. The full lines correspond to the emission of protons at $\theta = 70^\circ$ while the dashed ones correspond to protons emitted at $\theta = 70.5^\circ$ Each line corresponds to an emission point taken on a circonference with radius equal to 2 mm to simulate a beam spot size effect.

obtained using an array of detectors with a two dimensional measurement of the impact point. To infer the emission angle from the position on the detectors we used OPERA code to trace back to the target the proton emitted with fixed energy. The effect of the beam spot size on the emission angle reconstruction was estimated evaluating the

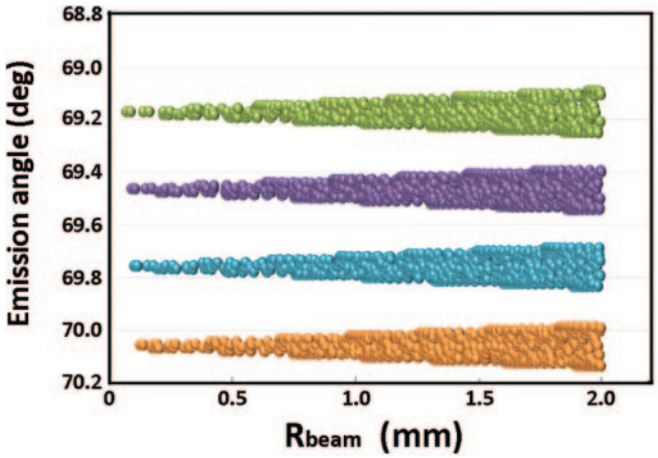

Fig. 5. – Proton emission angle recostructed from the impact point on the detector array as a function of the beam spot size. Calculations are shown for a beam spot size up to 2 mm radius.

range of polar angles corresponding to proton trajectories that intersect a defined beam spot size. In fig. 5 the recostructed emission angles as a function of the beam spot size are shown in the case of 4 MeV protons hitting the detector array at different impact points, 3 mm spaced in z and at the center of the lateral extent of the detectors. A clean separation of the reconstructed angles is observed. With increasing the beam spot size from zero to 2 mm the indetermination increases but remains still limited to about 0.15 degrees (see fig. 5). If one adds events hitting the detector along the full lateral extent the indeterminations related to the beam spot size becomes about 0.3 degrees.

These preliminary results suggest the possibility to build a helical-orbit spectrometer using the SOLE field. Further simulations are needed to investigate the potentialities of such a device with the LNS radioactive beams. A test phase using a tandem beam to study a well-known reaction with a limited number of detectors is foreseen in the next future to evaluate the performances of the spectrometer.

4. – Conclusions

An important upgrade phase of the superconducting cyclotron and the fragment separator is under way at the Laboratori Nazionali del Sud in Catania. To fully exploit the potentialities of the new facility an upgrade of the existent detector systems (CHIMERA, MAGNEX) is ongoing together with the development of new detectors systems like FARCOS. A feasibility study to use the magnetic field of SOLE solenoid to buid an helical orbit spectrometer to be used with RIBs delivered by the new facility has been undertaken in the last years. Preliminary results suggest the feasibility of such a spectrometer using a not homogeneous field coupled to an array of bidimensional position sensitive silicon detectors. Further simulations are needed to fully explore the performances of this device and its possible applications.

REFERENCES

[1] Calabretta L. *et al.*, *Mod. Phys. Lett. A*, **32** (2017) 1740009.
[2] Raciti G. *et al.*, *Nucl. Instrum. Methods B*, **266** (2008) 4632.
[3] Russotto P. *et al.*, *J. Phys.: Conf. Ser.*, **1014** (2018) 012016.
[4] Cappuzzello F. *et al.*, *Eur. Phys. J. A*, **54** (2018) 72.
[5] Cappuzzello F. *et al.*, *Eur. Phys. J. A*, **52** (2016) 167.
[6] Pagano E. V. *et al.*, *EPJ Web of Conferences*, **117** (2016) 10008.
[7] Pagano A. *et al.*, *Nucl. Phys. News*, **22** (2012) 28 and references therein.
[8] Bellia G. *et al.*, *IEEE Trans. Nucl. Sci.*, **43** (1996) 1737.
[9] Migneco E. *et al.*, *Nucl. Instrum. Methods A*, **314** (1992) 31.
[10] Anne R. *et al.*, *Nucl. Instrum. Methods A*, **257** (1987) 215.
[11] Tarasov O. B. and Bazin D., *Nucl. Instrum. Methods B*, **376** (2016) 185.
[12] Woosmaa A. H. *et al.*, *Nucl. Phys. A*, **746** (2004) 267c.
[13] Woosmaa A. H. *et al.*, *Nucl. Instrum. Methods A*, **580** (2007) 1290.
[14] Cobham, Vector Field Ltd., *Opera-3D reference manual*, UK.